

Bender Elements: Performance and Signal Interpretation

Jong-Sub Lee¹ and J. Carlos Santamarina²

Abstract: Bender elements are convenient shear wave transducers for instrumenting soil cells due to optimal soil–transducer coupling and compatible operating frequency. Experimental and analytical methods are implemented in this study to explore various aspects of bender element installations including: electromagnetic coupling prevention, directivity, resonant frequency, detection of first arrival, and near field effects. It is shown that electromagnetic coupling effects are critical in soils with high electrical conductivity and can be minimized by shielding and grounding, or by using parallel-type bender elements. Bender elements generate both P- and S-waves. The in-plane S-wave directivity is quasircular. The resonant frequency of bender element installations depends on the geometry of the bender element, the anchor efficiency, and the soil stiffness. The cross correlation of subsequent reflections is a self-healing measurement procedure which resolves uncertainties in both travel time and travel distance. Near field effects can be effectively taken into consideration by matching the measured signal with the analytical solution, directly rendering shear wave velocity.

DOI: 10.1061/(ASCE)1090-0241(2005)131:9(1063)

CE Database subject headings: Analytical techniques; Coupling; Resonance; Signal processing; Shear waves; Wave reflection.

Introduction

The small-strain shear modulus G_{\max} provides valuable soil information, which is relevant to a wide range of engineering tasks including the design of foundations subjected to dynamic loading, process monitoring, liquefaction assessment, and soil improvement control. The value of G_{\max} can be obtained from shear wave velocity measurements using piezoelectric transducers.

Jacques and Pierre Curie discover the phenomenon of piezoelectricity in 1880. By the late 1940s, different studies find that a ceramic substance can be polarized and made piezoelectric. Soon afterwards, piezoelectric properties are observed in lead–zirconate–titanate (PZT). Piezoelectricity results from lack of crystal symmetry or from the electrically polar nature of crystals. When a mechanical load is applied to a piezo material, the lattice distorts the dipole moment of the crystal and a voltage is generated; the voltage output increases with crystal asymmetry. On the other hand, when a voltage is applied, the crystal deforms. The sign of the voltage output or the direction of the mechanical deformation depends on the poling or polarization direction of the crystal.

Standard S-wave piezoelectric transducers are not adequate to measure shear wave velocity in soils due to weak S-wave directivity, poor coupling with the soil, high operating frequency,

and/or high impedance mismatch. Bender elements resolve these problems. A bender element is a thin, two-layer plate that can be installed in most soil cells. Shirley and Hampton (1978) and Shirley (1978) introduce bender elements to soil testing. Later, Dyvik and Madshus (1985) show the agreement between G_{\max} measured with bender elements and resonant column.

There are several difficulties associated with bender element installations, including electrical crosstalk due to electromagnetic coupling through the soil, mixed radiation of both P- and S-waves, near field effects, and uncertain detection of first arrivals. These are addressed next.

Electromagnetic Coupling—Crosstalk

The bender element is a two-layer piezoelectric transducer that consists of two conductive outer electrodes, two piezoceramic sheets, and a conductive metal shim at the center [Fig. 1(a)]. The outer electrodes are typically made of deposited nickel or silver. There are two types of bender elements: series and parallel. In the series type, the poling directions of the two piezoelectric layers are opposite to each other and the bender element is connected at the outer electrodes shown in Fig. 1(b). In the parallel type, the two piezoelectric layers have the same poling direction as shown in Fig. 1(c), the ground cable is attached to both outer electrodes, and the core wire is connected to the intermediate metal shim. For the same applied voltage, the parallel-type connection provides twice the displacement of the series-type connection. Therefore, manufacturers often recommend the use of parallel-type bender elements as source and the series-type bender elements as receiver.

Electromagnetic coupling between source and receiver bender elements manifests as an output signal with an early component that is quasisimultaneous with the input signal. This “crosstalk” can be very important in conductive soils such as wet clays on seafloor sediments. An experimental study is designed to explore crosstalk in series and parallel-type bender elements. These and all other measurements documented in this manuscript are con-

¹Assistant Professor, Dept. of Civil and Environmental Engineering, Korea Univ., Seoul 136-701, Korea; formerly, Georgia Institute of Technology.

²Professor, Dept. of Civil and Environmental Engineering, Georgia Institute of Technology, Atlanta, GA 30332 (corresponding author). E-mail: carlos.santamarina@ce.gatech.edu

Note. Discussion open until February 1, 2006. Separate discussions must be submitted for individual papers. To extend the closing date by one month, a written request must be filed with the ASCE Managing Editor. The manuscript for this paper was submitted for review and possible publication on January 25, 2004; approved on December 7, 2004. This paper is part of the *Journal of Geotechnical and Geoenvironmental Engineering*, Vol. 131, No. 9, September 1, 2005. ©ASCE, ISSN 1090-0241/2005/9-1063–1070/\$25.00.

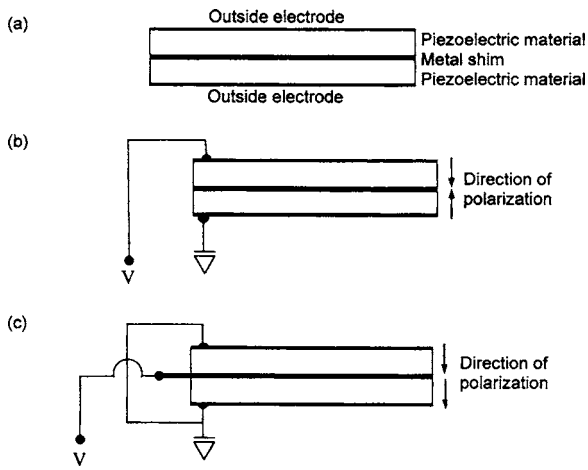


Fig. 1. Bender elements: (a) schematic representation of bender element, (b) series type, and (c) parallel type

ducted with $12.7 \times 8.0 \times 0.6$ (length \times width \times thickness in millimeters) PZT bender elements. All bender elements are water proofed with a thin polyurethane coat. Series-type bender elements are electrically shielded with conductive paint applied on top of the polyurethane layer, and then grounded.

Fig. 2(a) shows typical crosstalk effects observed with two series-type bender elements without grounding; the received signal resembles the discharge of a capacitor. Crosstalk can be effectively removed by grounding either the source or the receiver

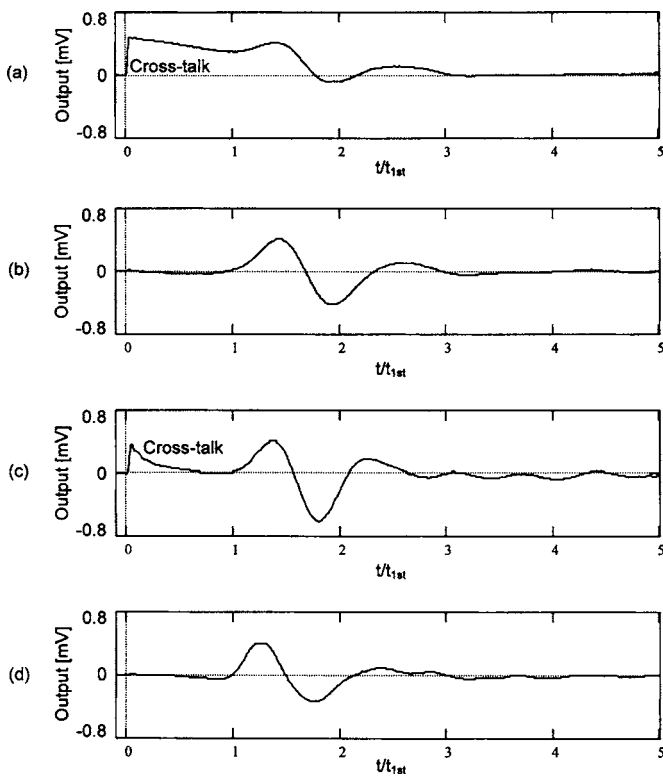


Fig. 2. Crosstalk effects: (a) series-to-series without grounding; (b) series-to-series with shielding and grounding; (c) parallel-to-series without shielding and grounding; and (d) parallel-to-parallel without shielding. Time “ t_{1st} ” corresponds to S-wave first arrival (input: step signal, tip-to-tip distance: $L=100$ mm).

[Fig. 2(b)]. The outer electrodes in a parallel-type connection have a shielding effect when connected to ground. Still, crosstalk can be observed in the series-to-parallel combination when the series element is not shielded and grounded [Fig. 2(c)]. Crosstalk vanishes when two parallel-type bender elements are used [Fig. 2(d)]. Note: external electrodes on both elements are connected to ground). Nevada sand is used for this study ($D_{50}=0.16$ mm, $e_{max}=0.87$, $e_{min}=0.54$).

Directivity

The transverse and in-plane directivity of bender elements (sources and receivers) affect S-wave measurement in instrumented cells, such as oedometers and triaxials, and other applications including tomographic monitoring systems.

Transverse Directivity

Bender elements generate two P-wave side lobes normal to their plane (one in compression and the other in rarefaction), and an S-wave frontal lobe as shown in Fig. 3(a). The ratio between the P- and S-wave velocities is

$$\frac{V_P}{V_S} = \sqrt{\frac{2(1-\nu)}{1-2\nu}} \quad (1)$$

For dry or unsaturated soils, Poisson’s ratio $\nu \approx 0.1$ and the $V_P/V_S \approx 1.5$. For saturated soils, V_P/V_S is stress dependent and it may exceed 20 for soils subjected to low effective stress. P-waves reflected from cell walls may interfere with the S-wave arrival. P

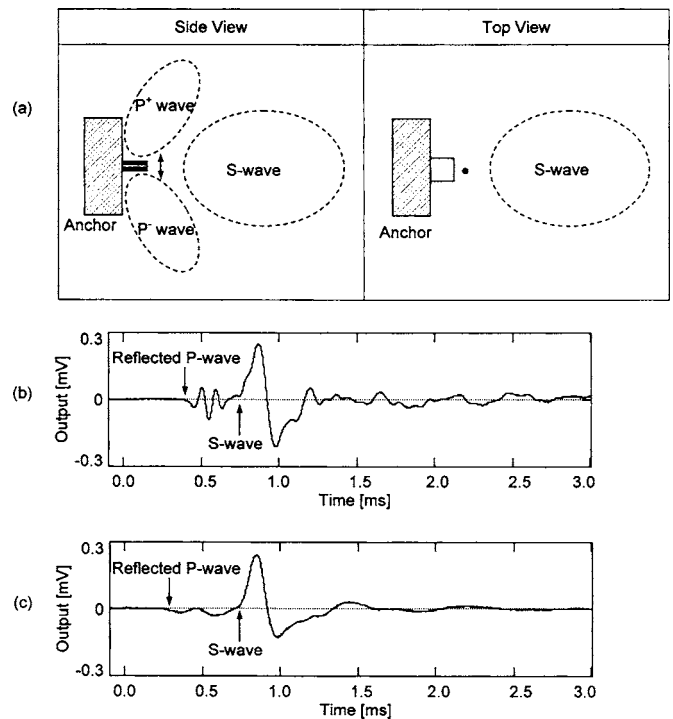


Fig. 3. Directivity of bender element and consequences of transverse directivity on measured signals: (a) transverse and in-plane directions; (b) and (c) measured signals in dry specimen and partially saturated specimen (input: 2.5 V step signal. Tip-to-tip distance: $L=32$ mm; oedometer cell diameter=70 mm).

and S signal interference depends on cell geometry and V_p/V_s ratio, i.e., state of stress and saturation conditions. Figs. 3(b and c) show P-wave interference in a dry specimen and after submerging it (partial saturation). The P-wave reflected from the cell wall arrives earlier than the direct S-wave; this is not a near field effect. Interference problems can be disregarded when the P-wave arrives significantly earlier than the S-wave. Note that reversing the polarity of the input excitation causes polarity reversal in both the direct S-wave as well as the reflected P-wave. A bender element source also generates a signal at the anchor; in the absence of isolation or mechanical impedance traps, this signal reaches the receiver traveling along cell walls. Reflected P-waves and wall signals in a cell can be studied by testing the cell in air and filled with water without soil.

In-Plane Directivity

Broad angular coverage is required for diagonal measurements. The in-plane directivity of bender elements is explored for two potential configurations shown in Fig. 4(a). The tip-to-tip distance from the source to each receiver is fixed (150 mm) to prevent geometric attenuation effects. A step signal is used as input. Directivity is established in terms of the peak amplitude. Measured values are plotted in Fig. 4(b), and fitted with a second order Fourier series. The deviation from circular directivity is more pronounced when the axes of the source and receiver bender elements are parallel to each other, such as in crosshole installations. The amplitude in the transverse configuration is about 75% of the amplitude at 0° in the parallel axes configuration. Overall,

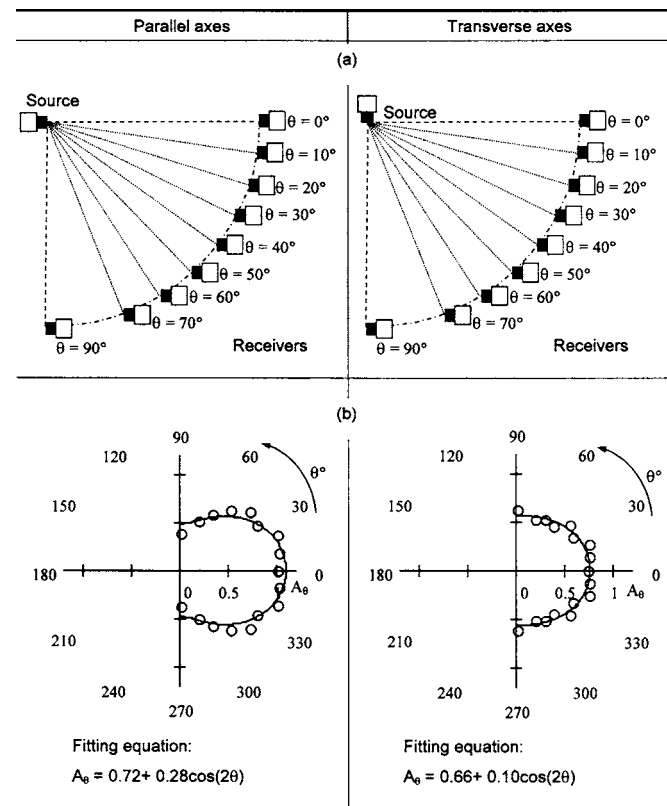


Fig. 4. Source–receiver directivity: (a) test setup, and (b) polar plot of peak amplitudes. Data points are duplicated by invoking symmetry. Amplitudes are normalized by amplitude at 0° in parallel axes configuration (input: step signal, tip-to-tip distance: $L=150$ mm).

these results suggest the potential use of bender elements in a wider range of in-plane configurations besides the standard tip-to-tip alignment, including data intensive tomographic applications.

Resonant Frequency

The resonant frequency of bender elements affects the size of the near field, travel time determination, resolution, and skin depth. Therefore, the resonant frequency is an important design parameter for bender element installations.

Bender Element in Air: Cantilever Beam

A bender element in air is equivalent to a cantilever beam. The resonant frequency of a cantilever beam is a function of the elastic modulus E_b , the moment of inertia I , and the mass per unit length \bar{m} . For a fixed–free boundary condition (displacement and slope are zero at the fixed end; moment and shear force are zero at the free end), the resonant frequency for the first mode is (Meirovitch 1967)

$$f_r = \frac{\omega}{2\pi} = \frac{1}{2\pi} \sqrt{\frac{k_b}{m_b}} = \frac{1}{2\pi} \sqrt{\frac{1.875^4 E_b I}{\bar{m}(\alpha L_b)^4}} \quad (2)$$

where k_b =equivalent spring constant; $m_b = \bar{m}L_b$ =cantilever mass; L_b =cantilever length; and α =effective length factor which is affected by the anchor efficiency ($\alpha=1$ for a perfectly rigid anchor and $\alpha > 1$ for a soft anchor). Note that the equivalent spring constant of the beam is $k_b = 1.875^4 E_b I / (\alpha L_b)^3$.

The mass of a bender element is $m_b = \rho_b b t (\alpha L_b)$, where b and h are the width and thickness. Typically, for piezoceramic materials $E_b = 6.2 \times 10^{10}$ N/m² and $\rho_b = 7,500$ kg/m³. After these properties are substituted into Eq. (2), the resonant frequency of an anchored bender element held in air is

$$f_r = 464 [\text{Hz} \cdot \text{m}] \frac{h}{(\alpha L_b)^2} \quad (3)$$

Bender Element in Soil

The resonant frequency of an anchored bender element buried in a soil mass is affected by the soil density and stiffness. The soil stiffness is obtained from Mindlin's solution for a point load within a continuum integrated to a rectangular geometry (Poulos and Davis 1974)

$$k_s = \eta E_s L_b \quad (4)$$

where $\eta \approx 2$ =mean displacement influence factor at the soil–element interface. The elastic modulus of the soil E_s can be calculated using the shear wave velocity V_s , Poisson's ratio ν , and the soil mass density ρ_s . Then, the equivalent spring constant of the soil mass becomes

$$k_s = 2\eta V_s^2 \rho_s (1 + \nu) L_b \quad (5)$$

The effective soil mass m_s is related to the $b^2 L_b$ volume

$$m_s = (\rho_s b^2 L_b) \beta \quad (6)$$

where β =experimentally determined value. Finally, a first-order estimate of the resonant frequency of a bender element in soil is herein obtained by combining the mass and stiffness of the bender element and the affected soil, resulting in an equivalent spring

constant $k_{eq} = k_b + k_s$ and an equivalent mass $m_{eq} = m_b + m_s$ [refer to Eq. (2)]

$$f_r = \frac{1}{2\pi} \left[\frac{1.875^4 \frac{E_b I}{(\alpha L_b)^3} + 2\eta V_s^2 \rho_s (1 + \nu) L_b}{\rho_b b h (\alpha L_b) + (\rho_s b^2 L_b) \beta} \right]^{1/2} \quad (7)$$

Experimental Study

The frequency response of anchored bender elements in air and in soil are measured using a Stanford Research Network Signal Analyzer (SR780). The bender element in air is excited with an impact and corroborated by laterally pushing the bender element with a 0.3 mm lead until the lead breaks in bending to simulate a negative step excitation. The resonant frequency of a bender element in soil is measured using an identical bender element pair where the source bender element is excited with a step input signal. In both cases, a mechanical, bolt-clamp anchoring system is used to facilitate adjusting the cantilever length.

Results

Analytically predicted and experimentally measured resonant frequencies in air and in soil are shown in Fig. 5. A salient feature in both experimental and analytical results is the crossing of “in soil” and “in air” trends. Results confirm that the resonant fre-

quency of bender element installations in soil depends on the soil stiffness (i.e., shear wave velocity), the stiffness of the bender element itself, and the cantilever length. The frequency is more dependent on bender element properties when the cantilever length is short. In this case, the resonant frequency in air is higher than the resonant frequency in soil. However, the frequency is controlled by soil properties when the cantilever length is long. In this case, the resonant frequency in air decreases rapidly with cantilever length, and it becomes smaller than that in soil.

The effective length factor α that corresponds to the mechanical bolt-anchor is obtained by fitting the model [Eq. (2)] to the data gathered with the bender element in air. The inferred value is $\alpha = 1.2$. The effective soil mass factor β is determined by fitting the data gathered for the bender element in soil with the model proposed in Eq. (7). The calculated effective soil mass factor is $\beta = 1.6$. Note that while both α and β carry physical meaning, their main role is to accommodate a simple model to a relatively complex system.

Fig. 6 shows the variation in resonant frequency for an epoxy anchored bender element. The soil stiffness is gradually increased by increasing the load applied onto the oedometer cap and it is captured in terms of shear wave velocity. The analytical trend corresponds to $\alpha = 1.5$ and $\beta = 1.6$. (The value of β determined in Fig. 5 is not changed for this analysis.) It is concluded that the effective length is longer in the softer epoxy-type anchor system. Data in Fig. 6 clearly show the effect of soil stiffness on the resonant frequency of bender element installations (see also data in Santamarina and Fam 1997).

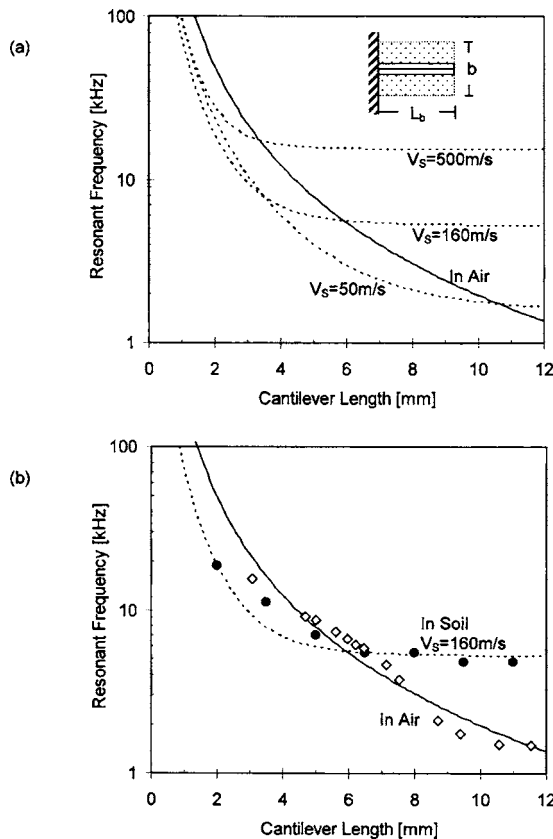


Fig. 5. Resonant frequency of bender elements in air and in soil: (a) analytical solution (mechanical, bolt-clamp anchor: $\alpha = 1.2$, $\beta = 1.6$), and (b) experimental results—solid and dotted lines correspond to the analytical solution; points are measured values. Applied effective vertical stress: 148 kPa.

Input and Output Signals

The electrical signal input to a bender element installation is convolved through a series of frequency response functions [Fig. 7(a)]: (1) H_{p-in} the input peripheral electronics such as power amplifiers and cables; (2) H_{be-in} the bender element-soil response at the source; (3) H_{soil} the soil; (4) H_{be-out} the bender element-soil response at the receiver; and (5) H_{p-out} the response of peripheral electronics at the output. For quasilinear soil behavior and adequate peripheral electronics, the measured global frequency response is strongly determined by the frequency response of the bender element-soil pair, i.e., $H_{be-in} \cdot H_{be-out}$.

Measured input and output signals for a given bender element

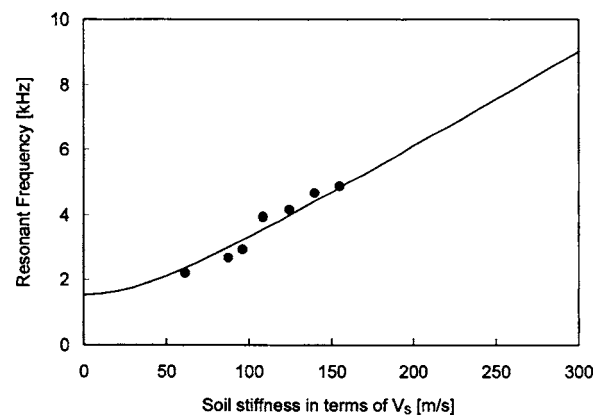


Fig. 6. Soil stiffness effects on resonant frequency. Circular points are experimental results with identical pair (cantilever length $L_b = 6.5$ mm, epoxy-type anchoring). Solid line corresponds to analytical solution for $\alpha = 1.5$ and $\beta = 1.6$

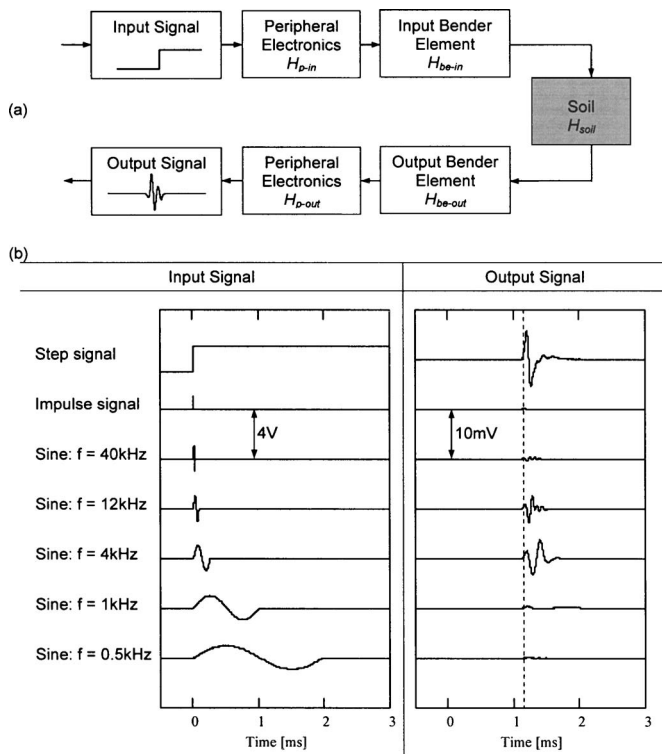


Fig. 7. Bender element installation: (a) sequence of frequency response functions; and (b) input and output signals. Tip-to-tip distance: $L=105$ mm, cantilever length: 6.5 mm, $V_S=93$ m/s. Resonant frequency of bender element $f_r=3.6$ kHz, $L/\lambda=4.0$.

installation are presented in Fig. 7(b). The bender element response is enhanced when the frequency of the input sine signal approaches the resonant frequency of the bender element–soil system (see also Jovicic et al. 1996; Kawaguchi et al. 2001). The first arrival is not affected by the selected input frequency, however, the ability to detect the arrival time can change dramatically.

The optimal single-period sinusoid is the one near the resonant frequency of the bender element installation at the given soil stiffness (the resonant frequency is readily assessed by sweeping the excitation frequency while observing the Lissajous response in the oscilloscope in the X – Y mode). Because a step input signal includes all frequencies, a clear response is measured regardless of soil stiffness. Therefore, the step input signal is advantageous when the resonant frequency is unknown or if it is expected to change rapidly during testing (as in liquefaction monitoring).

Shear Wave Velocity Determination by Multiple Reflections

Several difficulties such as the selection of travel distance, the determination of travel time, and near field effects affect the measurement of soil shear wave velocity using bender element installation. These issues are addressed next.

Travel Distance and Travel Time

There are conflicting guidelines for the selection of the travel length and travel time for shear wave velocity determinations with bender elements. The tip-to-tip distance is herein adopted and it is supported by data gathered with bender elements and

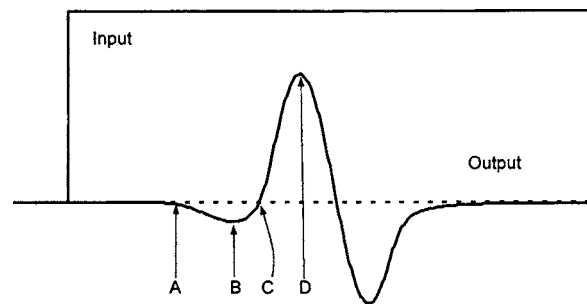


Fig. 8. Typical S-wave signal within near field ($L/\lambda=1$): (A) first deflection, (B) first bump maximum, (C) zero after first bump, and (D) major first peak

resonant column tests (Dyvik and Madshus 1985), data from travel time versus sample length studies (Viggiani and Atkinson 1995a), and multiray, length varying tomographic studies (Fernandez 2000).

The determination of the arrival time, on the other hand, is more controversial. A typical output signal gathered from a step input signal is presented in Fig. 8 (detected within the near field—see also Brignoli et al. 1996; Arulnathan et al. 1998). What is the first arrival A, B, C, or D? Suggested criteria and recommendations vary depending on installation, application, and input signal (Abbiss 1981; Dyvik and Madshus 1985; Mancuso et al. 1989; Fam and Santamarina 1995; Viggiani and Atkinson 1995a,b; Jovicic et al. 1996; Jovicic and Coop 1997; Santamarina and Fam 1997; Blewett et al. 1999; Lohani et al. 1999; Kawaguchi et al. 2001). Alternative signal processing procedures have been explored to avoid “picking” a travel time, including cross correlation and frequency domain analyses. However, such techniques must relate signals of the “same nature” or accommodate for the several frequency response functions identified in Fig. 7: only H_{soil} is wanted (see examples in Brocanelli and Rinaldi 1998; Blewett et al. 2000; Arroyo et al. 2003).

Solution of Travel Distance and Travel Length

Multiple reflections detected with the same bender element provides a simple yet robust method to overcome travel length and travel time uncertainties. The cell built to demonstrate this concept is designed to mechanically filter side lobe P-waves by using a large diameter cell (Fig. 9). The S-wave reflections from end plates are enhanced by maximizing the soil–plate impedance mismatch. In this study, bender elements are mounted into steel plates.

A typical signal measured with the receiving bender element is shown in Fig. 10(a). The cross-correlation between the first event $x(t)$ and the second event $z(t)$ detected with the same transducer is

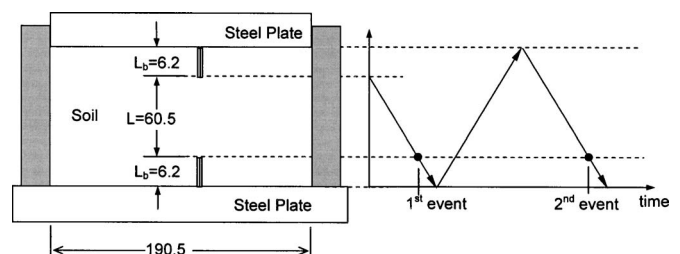


Fig. 9. Multiple-reflection method. All dimensions are in millimeters.

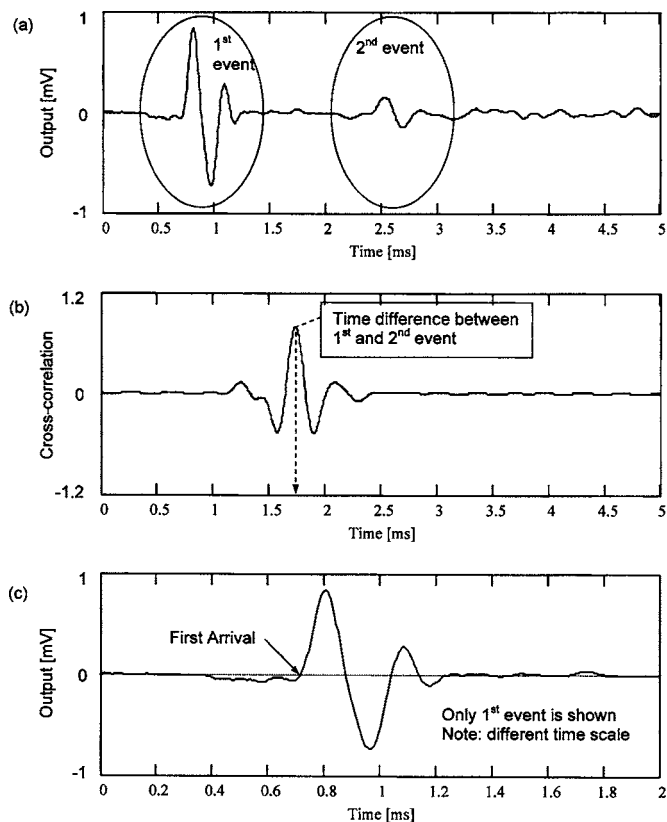


Fig. 10. Multiple reflection test results: (a) typical measured signal (first and second events are clearly measured); (b) cross-correlation peak corresponds to travel time—1.725 ms; and (c) first arrival of S-wave 0.715 ms. Tip-to-tip distance: $L=60.5$ mm.

computed to identify the travel time [Fig. 10(b)]: the travel time t_{cc} corresponds to the peak in the cross-correlation. This method solves uncertainty not only in travel time but also in travel distance: the travel distance between the first and second event is always twice the plate-to-plate distance $2(L+2L_b)$, as shown in Fig. 9. Then, shear wave velocity is

$$V_S = \frac{2(L+2L_b)}{t_{cc}} \quad (8)$$

The first arrival that is computed using this value of V_S and the tip-to-tip distance is denoted in Fig. 10(c). In this case, the first arrival corresponds to point C in Fig. 8. This suggests that small bumps ahead of the signal can be disregarded. (Note: it is anticipated that the early bump is input signal dependent as it relates to near field effects.)

Given that the two event signals $x(t)$ and $z(t)$ are measured with the same transducer, the frequency response between them $H(\omega)=\text{FFT}[z(t)]/\text{FFT}[x(t)]$ automatically cancels all the peripheral effects [bender element frequency response, crystal-soil coupling, and electronics—Fig. 7(a)], therefore $H(\omega)=H_{\text{soil}}$ (see self healing measurements in Fratta and Santamarina 1996). Then, frequency dependent travel time and dispersion effects can be explored with the unwrapped phase $\phi(\omega)=\arctan[\text{Im}(H_{\text{soil}})/\text{Re}(H_{\text{soil}})]$

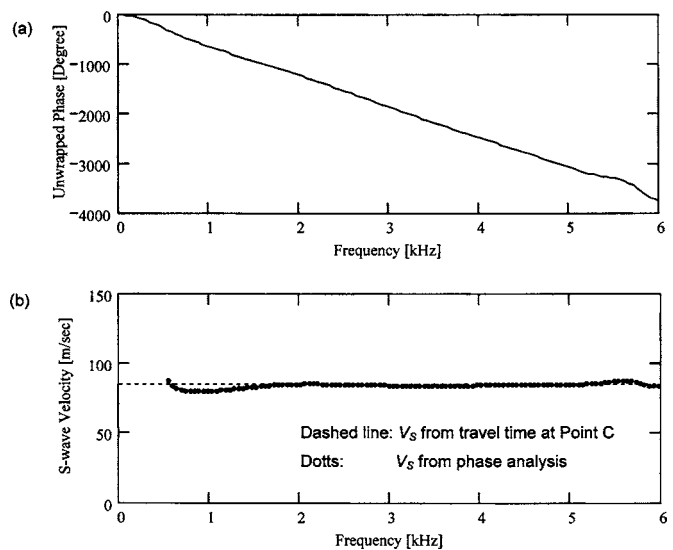


Fig. 11. Phase analysis in multiple reflection method: (a) unwrapped phase; and (b) S-wave velocity spectrum

$$t(\omega) = \frac{\phi(\omega)}{\omega} \quad (9)$$

The unwrapped phase and the velocity spectrum are shown in Fig. 11.

Shear Wave Velocity Determination in Near Field

Cruse and Rizzo (1968) obtained the analytical general solution for wave motion within an infinite isotropic elastic medium for a point source with axial displacement. The solution involves both longitudinal and transverse motions in space and applies to both the near and far fields. In three dimensions, the solutions for the longitudinal motion (P-motion) and transverse motion (S-motion) were derived from the general solution by Sanchez-Salinerio et al. (1986) (see Aki and Richards 1980 for a general solution and Arroyo et al. 2003 for a detailed discussion in the context of bender elements). This analytical solution permits exploring a “signal-matching” method to extract the shear wave velocity from measurements with pronounced near field effects. The method consists of gradual changing the unknown model parameters to match the measured waveforms. The mathematical formulation and the recommended step-by-step procedure for signal matching are summarized in Table 1.

Fig. 12 shows measured waveforms S_{meas} (dotted lines) and analytically calculated waveforms S_{cal} (solid lines) during an oedometer-loading and unloading test of Nevada sand. The electrical input signal is a step but a single period sinusoid is assumed for matching on the basis of the step response shown in Fig. 7. Matching is emphasized for the early part of the signal. Given the various unknown parameters in the solution, besides V_S , the implementation of this methodology is more robust when a family of signals is available, as in the example shown in Fig. 12.

Fig. 13 shows a comparison between the values of V_S obtained from the signal matching technique and those obtained from the travel time at point C (refer to Fig. 8) for all signals presented in Fig. 12. The difference between these two procedures is about 1% for this dataset. As discussed earlier, proper data interpretation is needed in each case.

Table 1. Signal Matching Procedure

Step	Description and formulation
1	Determine geometric parameters: The tip-to-tip distance L between bender elements Their relative out-of plane misalignment φ
2	Measure the signal $S_{meas}(t)$. Estimate resonant frequency f_r and shear wave velocity V_s
3	Define the input signal radiated by the bender element $x(t)$, such as wavelet or a single period sinusoid with period $1/f_r$.
4	Compute the Fourier transform of the input signal $X(\omega)$ $=FFT[x(t)]$
5	Compute the 3D wave motion corresponding to an impulse (frequency domain)
	P motion:
	$U(\omega) = \frac{1}{4\pi\rho(V_s^*)^2} [\Gamma(\omega) - \Xi(\omega)]$
	S motion:
	$V(\omega) = \frac{1}{4\pi\rho(V_s^*)^2} \Gamma(\omega)$
	where
	$\Gamma(\omega) = \left[1 + \frac{V_s^*}{j\omega L} - \left(\frac{V_s^*}{\omega L} \right)^2 \right] \frac{e^{-j\omega L/V_s^*}}{L} - \left(\frac{V_s^*}{V_p^*} \right)^2 \left[\frac{V_p^*}{j\omega L} - \left(\frac{V_p^*}{\omega L} \right)^2 \right] \frac{e^{-j\omega L/V_p^*}}{L}$
	$\Xi(\omega) = \left[1 + 3 \frac{V_s^*}{j\omega L} - 3 \left(\frac{V_s^*}{\omega L} \right)^2 \right] \frac{e^{-j\omega L/V_s^*}}{L} - \left(\frac{V_s^*}{V_p^*} \right)^2 \left[1 + 3 \frac{V_p^*}{j\omega L} - 3 \left(\frac{V_p^*}{\omega L} \right)^2 \right] \frac{e^{-j\omega L/V_p^*}}{L}$
	complex shear wave velocity $V_s^* = V_s(1 + jD)$; damping D ; and $j^2 = -1$
6	Convolve the input signal with the frequency response for P and S
	P-wave signal: $Y_P(\omega) = U(\omega) \cdot X(\omega)$ S-wave signal: $Y_S(\omega) = V(\omega) \cdot X(\omega)$
7	Compute the inverse Fourier transform of $Y_P(\omega)$ and $Y_S(\omega)$ to determine the P and S-wave time series
	P-wave: $y_p(t) = IFFT[Y_P(\omega)]$ S-wave: $y_s(t) = IFFT[Y_S(\omega)]$
8	Correct the predicted S-motion for out-of plane misalignment φ
	$S_{cal}(t) = y_p(t) \sin \varphi + y_s(t) \cos \varphi$
9	Compare $S_{meas}(t)$ and $S_{cal}(t)$
10	Modify V_s and repeat from Step 5 until an adequate match is obtained
	Other parameters may also require adjusting (within physically acceptable ranges)
	The value of V_s is the most significant parameter for time shift control.

Notes: 1-If both bender elements are on the same plane, $\varphi=0$.

2-The damping D is a "system damping," and it includes installation and coupling effects at both bender elements, directivity effects, and soil damping.

3-The solution requires V_p . It can be estimated from V_s and Poisson's ratio. V_p must be measured in applications where the soil saturation is changing.

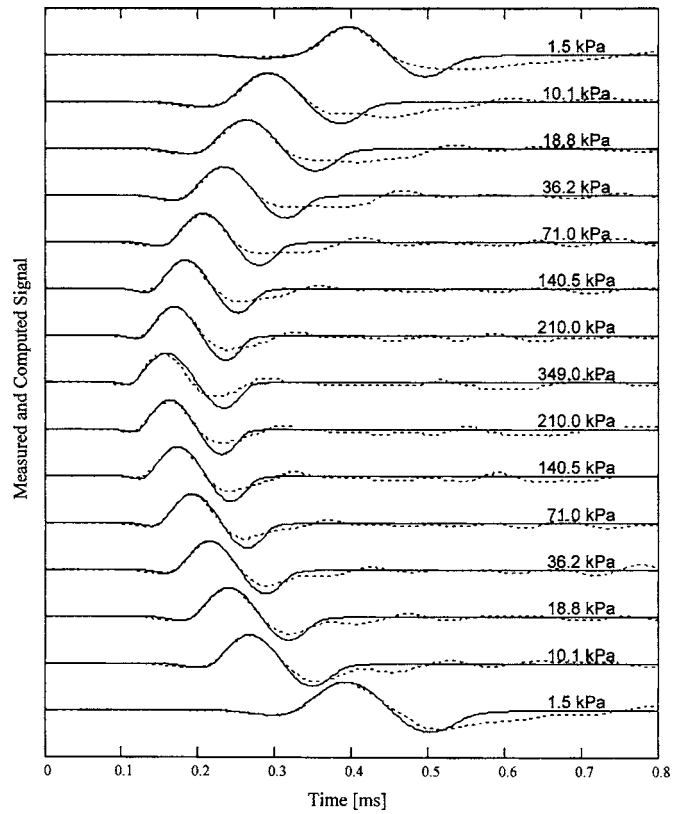


Fig. 12. Identifying value of V_s in presence of near field effects by signal matching technique: (dotted line) measured signals; (solid line) computed signals. Numbers on right side indicate applied vertical effective stress. Each measured signal is normalized by its maximum value. Signals predicted following simulation procedure in Table 1 assume constant input amplitude. Tip-to-tip distance before consolidation: $L=19.80$ mm, oedometer cell diameter=100 mm.

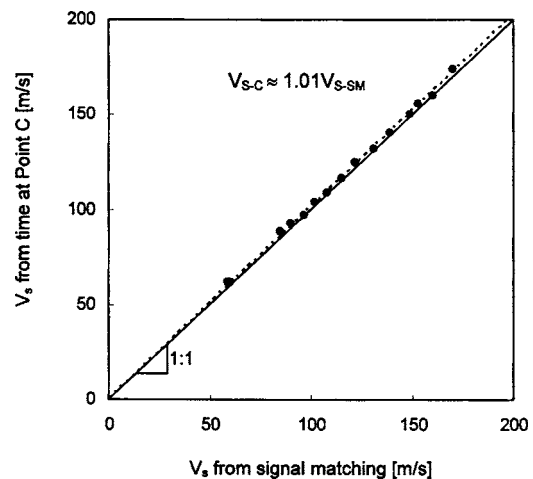


Fig. 13. Comparison between shear wave velocity V_{s-C} computed with first arrival at point C (refer to Fig. 8) and shear wave velocity V_{s-SM} obtained with signal matching technique—time series shown in Fig. 12

Conclusions and Recommendations

Experimental and analytical methods are implemented to study electromagnetic coupling, directivity, resonant frequency, frequency response, near field effects, and first arrival detection. The main observations from this study are as follows:

1. Electromagnetic coupling between source and receiver bender elements is enhanced in soils with high electrical conductivity. Crosstalk effects can be minimized by shielding and grounding. A grounded parallel-type bender element pair effectively reduces crosstalk.
2. Bender elements exhibit both transverse and in-plane directivity. The arriving S-wave interferes with radiated side-lobe P-waves that reflect from cell walls. Therefore, the specimen radius-to-height ratio must be accounted for in experimental design. The in-plane directivity is quasicircular and allows for both side-to-side (crosshole) and top-to-side installations.
3. An installed bender element is a cantilever beam. Once it is buried in a soil mass, the effective transducer is a complex system which combines both the bender element itself and the soil in its vicinity. The resonant frequency of the bender element in soil is bender element stiffness dependent for short cantilever lengths, and it is soil stiffness dependent for long cantilever lengths. As the resonant frequency depends on the soil stiffness, a higher frequency is obtained at higher effective stress.
4. Signal interpretation is facilitated when multiple reflections are used. This approach solves two issues simultaneously: the S-wave travel distance and arrival time. In this case, the travel distance is always twice the plate-to-plate distance, and the travel time corresponds to the cross-correlation peak. Multiple reflection signals can be properly analyzed in the frequency domain because all additional transfer functions cancel.
5. Matching experimental waveforms with the analytically computed waveforms facilitates shear wave velocity determination when signals are affected by near field effects.

Acknowledgment

This study was supported by the NSF-NEES project (based at the University of California at Davis and directed by Dr. B. L. Kutter and The Goizueta Foundation). The anonymous reviewers provided insightful comments and suggestions.

References

Abbiss, C. P. (1981). "Shear wave measurements of the elasticity of the ground." *Geotechnique*, 31(1), 91–104.

Aki, K., and Richards, P. G. (1980). *Quantitative seismology: Theory and method*, Freeman, New York.

Arroyo, M., Wood, D. M., and Greening, P. D. (2003). "Source near-field effects and pulse tests in soil samples." *Geotechnique*, 53(3), 337–345.

Arulnathan, R., Boulanger, R. W., and Riemer, M. F. (1998). "Analysis of

bender element tests." *Geotech. Test. J.*, 21(2), 120–131.

Blewett, J., Blewett, I. J., and Woodward, P. K. (1999). "Measurement of shear-wave velocity using phase-sensitive detection technique." *Can. Geotech. J.*, 36(5), 934–939.

Blewett, J., Blewett, I. J., and Woodward, P. K. (2000). "Phase and amplitude responses associated with the measurement of shear-wave velocity in sand by bender elements." *Can. Geotech. J.*, 37(6), 1348–1357.

Brignoli, E. G. M., Gotti, M., and Stokoe, K. H. II. (1996). "Measurement of shear waves in laboratory specimens by means of piezoelectric transducers." *Geotech. Test. J.*, 19(4), 384–397.

Brocanelli, D., and Rinaldi, V. (1998). "Measurement of low-strain material damping and wave velocity with bender elements in the frequency domain." *Can. Geotech. J.*, 35(6), 1032–1040.

Cruse, T. A., and Rizzo, F. J. (1968). "A direct formulation and numerical solution of the general transient elastodynamic problem." *J. Math. Anal. Appl.*, 22, 244–259.

Dyvik, R., and Madshus, C. (1985). "Lab measurements of G_{max} using bender element." *Proc., ASCE Convention on Advances in the Art of Testing Soils under Cyclic Conditions*, 186–196.

Fam, M. A., and Santamarina, J. C. (1995). "Study of geoprocesses with complementary wave measurements in an oedometer." *Geotech. Test. J.*, 19(4), 307–314.

Fernandez, A. L. (2000). "Tomographic imaging the state of stress." PhD thesis Civil Engineering, Georgia Institute of Technology, Atlanta.

Fratta, D., and Santamarina, J. C. (1996). "Wave propagation in soils: Multiple-mode, wide-band testing in waveguide device." *Geotech. Test. J.*, 19(2), 130–140.

Jovicic, V., and Coop, M. R. (1997). "Interpretation of bender element tests." *Geotechnique*, 47(3), 875.

Jovicic, V., Coop, M. R., and Simic, M. (1996). "Objective criteria for determining G_{max} from bender element tests." *Geotechnique*, 46(2), 357–362.

Kawaguchi, T., Mitachi, T., and Shibuya, S. (2001). "Evaluation of shear wave travel time in laboratory bender element test." *Proc., 15th Int. Conf. on Soil Mechanics and Geotechnical Engineering* 155–158.

Lohani, T. N., Imai, G., and Shibuya, S. (1999). "Determination of shear wave velocity in the bender element test." *Earthquake Geotechnical Engineering*, Seco and Pinto, eds., Lisboa, Portugal, 101–106.

Mancuso, C., Simonelli, A. L., and Vinale, F. (1989). "Numerical analysis of in situ S-wave measurement." *Proc., 12th Int. Conf. on Soil Mechanics and Foundation Engineering*, Rio de Janeiro, Brazil, 277–280.

Meirovitch L. (1967). *Analytical methods in vibrations*. Macmillan, New York.

Poulos, H. G., and Davis, E. H. (1974). *Elastic solutions for soil and rock mechanics*, Wiley, New York.

Sanchez-Salinerio, I., Rosset, J. M., and Stokoe, K. H. II. (1986). "Analytical studies of body wave propagation and attenuation." *Rep. No. GR-86-15*, Univ. of Texas, Austin, Tex.

Santamarina, J. C., and Fam, M. A. (1997). "Interpretation of bender element tests—discussion." *Geotechnique*, 47(4), 873–875.

Shirley, D. J. (1978). "An improved shear wave transducer." *J. Acoust. Soc. Am.*, 63(5), 1643–1645.

Shirley, D. J., and Hampton, L. D. (1978). "Shear wave measurements in laboratory sediments." *J. Acoust. Soc. Am.*, 63(2), 607–613.

Viggiani, G., and Atkinson, J. H. (1995a). "Interpretation of bender element tests." *Geotechnique*, 45(1), 149–154.

Viggiani, G., and Atkinson, J. H. (1995b). "Stiffness of fine-grained soil at very small strains." *Geotechnique*, 45(2), 249–265.